Polymer 50 (2009) 227–235

Contents lists available at ScienceDirect

Polymer

journal homepage: www.elsevier.com/locate/polymer

Rate dependent finite deformation stress–strain behavior of an ethylene methacrylic acid copolymer and an ethylene methacrylic acid butyl acrylate copolymer

S. Deschanel [a,*], B.P. Greviskes [a], K. Bertoldi [a], S.S. Sarva [a], W. Chen [c], S.L. Samuels [d], R.E. Cohen [b], M.C. Boyce [a]

[a] Department of Mechanical Engineering, Massachusetts Institute of Technology, 77 Massachusetts Avenue, Cambridge, MA 02139, United States
[b] Department of Chemical Engineering, Massachusetts Institute of Technology, United States
[c] Schools of Aeronautics and Astronautics and Materials Engineering, Purdue University, West Lafayette, IN 47907, United States
[d] E.I. du Pont de Nemours and Company, Inc., Wilmington, DE, United States

ARTICLE INFO

Article history:
Received 11 August 2008
Received in revised form
22 October 2008
Accepted 23 October 2008
Available online 5 November 2008

Keywords:
Ionomers
Stress–strain behavior
Rate dependence

ABSTRACT

The large strain deformation behaviors of an ethylene methacrylic acid (EMAA) copolymer and an ethylene methacrylic acid butyl acrylate (EMAABA) copolymer are evaluated and compared in compression over nearly eight orders of magnitude in strain rate, from 10^{-4} to almost 10^{4}/s. Transition regimes are quantified using dynamic mechanical analysis. The stress–strain behavior of these copolymers exhibits a relatively stiff initial behavior followed by a rollover to a more compliant response. The low strain modulus, the rollover stress and the large deformation stress–strain behavior are strongly dependent on strain rate. The proximity of the material glass transition to the room temperature test conditions results in a substantial change in the nature of the rate sensitivity of the stress–strain behavior as one moves over the range of strain rates. The mechanical behavior of the EMAA is contrasted to that of a corresponding EMAABA terpolymer and to its sodium-neutralized counterpart ($EMAABA_{Na}$). The nature of the rate sensitivity of the room temperature stress–strain behavior of EMAA transitions from a behavior near the glassy end of the leathery regime at low rates to a near glassy behavior at high rates. The butyl acrylate content in the EMAABA lowers the glass transition temperature and leads to a more compliant mechanical behavior (reduced initial stiffness, reduced rollover stress, reduced post-rollover stress level) at room temperature. The EMAABA behavior transitions from a rubbery-like behavior at the lowest rates to a leathery-like behavior at the highest rates. Upon sodium neutralization, the overall stiffness and flow stress levels are enhanced likely due to the presence of the ionic aggregates; the glass transition of $EMAABA_{Na}$ is broadened in comparison to the EMAABA, giving a rate dependent room temperature behavior that transitions through the leathery regime with increasing strain rate. A constitutive model that separately accounts for the distinct deformation resistances of the crystalline domains and the amorphous domains is able to capture the changes in rate dependent deformation behavior of the EMAA copolymers studied herein. The crystalline domains provide resistance to flow across a wide window in rate and temperature whereas the amorphous domains provide increasing resistance as the strain rate is increased and the material effectively transitions through the glass transition regime, providing a mechanism for changing rate sensitivity.

1. Introduction

Ethylene methacrylic acid (EMAA) copolymers are precursor materials for ionomers, in which the pendant acid groups are partially or fully neutralized with a metal cation such as sodium, magnesium, or zinc. The mechanical properties of ionomers exhibit a remarkable range in mechanical behavior depending on the microstructure of amorphous domains, ionic aggregates, and crystalline domains and their relative amounts in the overall material [1–3]. Changes in structure and properties strongly depend on the type and concentration of ionic groups distributed along the polymer chain backbone [4]. Various physical measurements have been carried out for several types of ionomers and different models [5–7] have been developed for the

* Corresponding author. Tel.: +33 4 72 43 81 84; fax: +33 4 72 43 79 30.
E-mail address: stephanie.deschanel@insa-lyon.fr (S. Deschanel).

0032-3861/$ – see front matter © 2008 Elsevier Ltd. All rights reserved.
doi:10.1016/j.polymer.2008.10.049

morphology of ionomers emphasizing the presence of small nanoscale aggregates uniformly distributed throughout the amorphous regions. At low ion content, the ion pairs form aggregates known as multiplets [5,8] and the effect of this entity is similar to that of a physical cross-link. As the ion content increases, sizeable ionic clusters develop which act not only as cross-links but also as micro-crystallites. These clusters have been observed in small-angle X-ray scattering [9]. Various physical properties, including mechanical properties and relaxation behavior, are dependent upon the microstructures that are formed [4,10]. A number of studies have been performed on the dynamic mechanical properties of the ethylene ionomers. MacKnight et al. [10] found several loss peaks for sodium-neutralized EMAA. In order of increasing temperature, the γ-peak occurs at ~−120 °C and is essentially the same as that found in ethylene homopolymers. Then, if the neutralization is greater than ~35% [10–13], a β peak is present at ~−10 °C and a higher temperature peak at ~50 °C is labeled "C" [14], representing the predominantly ionic microphase. While the ion-poor regions are responsible for the β relaxation, devitrification of the ion-rich regions contributes to the C relaxation; however its observation and interpretation are complicated by the simultaneous melting of secondary crystals [14]. The β relaxation would reflect the glass transition of ion depleted domains (i.e., unneutralized copolymer) within the amorphous phase [1,11,12], consistent with the restricted mobility model (RM) [5]. In some cases, the β and C peaks overlap in what is often called β′-transition.

Despite the large number of earlier studies, relatively little research has explored the deformation behavior of these semi-crystalline ionomers at large deformation and at very high strain rates (a study has been conducted on impact fracture behavior [15]). In this paper, we study an unneutralized ethylene methacrylic acid (EMAA) copolymer with 9% methacrylic acid, its counterpart 23% butyl acrylate (EMAABA) terpolymer and a 53% sodium-neutralized ethylene 9%-methacrylic acid 23%-butyl acrylate ($EMAABA_{Na}$) ionomer. These three different copolymers are studied in large deformation uniaxial compression over a wide range of strain rates (from 10^{-4}/s to 6.10^3/s). The viscoelastic relaxation mechanisms are determined using dynamic mechanical analysis; for each material, the shifting of the glass transition mechanism is then respectively correlated to the strong rate dependence observed for the large deformation stress–strain behavior.

2. Experimental section

2.1. Materials

The base EMAA used in this study contains 9 wt% methacrylic acid. The EMAABA ethylene copolymer resin contained 9% methacrylic acid (MAA) and 23% *n*-butyl acrylate (nBA). The EMAABA terpolymer was partially neutralized with sodium ions (53% of the acid groups neutralized by Na^+) to produce an ionomer referred to herein as $EMAABA_{Na}$. These random copolymers with long chain branches were produced using a high pressure autoclave process. The nature of the branching in their polyethylene sections is assumed to be similar to what is found in polyethylene homopolymers [16,17] produced via this process. All samples were provided by DuPont in the form of optically transparent compression molded plaques, nominally of thickness ~3.15 mm. For compression testing, three separate specimen sets were punched from these plaques. The first set consisted of 6 mm cylindrical specimens, punched using Miltex sterile disposable biopsy punches, and used for low rate testing. The second consisted of 6 mm cylindrical specimens punched using a special expulsion punch fabricated by Dewes-Gumbs Die Co, also used in low rate testing. The third used a similar expulsion punch, 5 mm in diameter; these specimens were used exclusively for high rate testing.

2.2. Instrumentation

2.2.1. Thermal and morphological characterization

Dynamic mechanical analysis (DMA) was performed on a TA Instruments Q800 DMA to obtain storage and loss moduli as a function of frequency and temperature. Rectangular specimens (approximately 20 mm × 3 mm × 2 mm) or cylindrical samples with a diameter of 2.5 mm and a length of 20 mm were tested in the cantilever and tensile mode in DMA with a fixed displacement of 15 μm. The testing temperature ranged from −150 to 50 °C with a 2 °C/min heating rate at frequencies of 1, 10, and 50 Hz. The particular frequencies of these tests were converted to corresponding average strain rates [18], giving a range in strain rate from $3(10^{-3})$ to $3(10^{-1})$/s (note that the same frequency may lead to different effective strain rates, owing to changes in sample geometry, the maximum strain amplitude achieved, etc.). Since the storage and loss moduli are frequency-dependent, converting the frequencies to corresponding strain rates allows us to relate the DMA data to the compression testing results.

Differential scanning calorimetry tests were performed either on a Thermal Advantage DSC Q1000 (TA Instruments, Inc.) or on a Pyris Diamond apparatus from Perkin–Elmer. All measurements were taken from −80 °C to 170 °C, with a temperature ramp rate of 10 °C/min.

2.2.2. Compression testing

Uniaxial compression tests were performed over a wide range of strain rates: 10^{-4}/s to nearly $6(10^3)$/s. Low to moderate rate compression testing (10^{-4}–10^{-1}/s) was accomplished on a Zwick mechanical tester (Zwick Roell Group). To reduce friction, thin Teflon films were placed between the specimen and the compression platens, and WD-40 lubricant was sprayed between Teflon films and platens. Moderate rate compression testing (1–10^2/s) was conducted at Purdue University on a servo-hydraulic MTS 810 machine. During low to moderate rate compression tests, a constant engineering strain rate was applied to a final true compressive strain of −1 (true strain is taken to be $\ln(l/l_0)$ with l being current sample height and l_0 being initial sample height; engineering strain is taken to be $\Delta l/l_0$). High strain rate tests ($2(10^2)$–10^3/s) were conducted on a long split Hopkinson pressure bar at Purdue University. The specimens for low to moderate rate compression tests were circular cylinders with diameter of 6 mm and height of 3 mm. Very high strain rate compression testing (>10^3/s) was conducted on a split Hopkinson pressure bar (SHPB) apparatus at MIT as described by Mulliken and Boyce [19]. Specimens for high rate testing were smaller circular cylinders with diameter 5 mm and height 2.5 mm to meet the particular requirements of this test. Specimens were lubricated with a thin layer of petroleum jelly on each surface prior to testing. As in the study of Sarva et al. [20], the comparison of the trend of the engineering strain rate to that of the corresponding true strain rate shows the engineering strain rate to be relatively constant over the course of a test while the true strain rate may increase by a factor of 2 for the highest rate tests. Noting that the strain rate varies over the course of a high rate test, each true stress–true strain curve will be identified by its true strain rate taken at a true strain of 0.50. In plots of stress versus strain rate, where the stress level is taken at different strains, the strain rate used is the rate at the particular value of strain. Following Garg et al. [21], due to the adiabatic conditions during high rate testing, the specimen temperature was also measured during the high rate SHPB tests using a customized infrared measurement capability.

3. Results

3.1. Dynamic mechanical analysis

3.1.1. Ethylene methacrylic acid copolymer without neutralization (EMAA)

Storage modulus, loss modulus and loss tangent curves of the EMAA are shown in Fig. 1 at a converted strain rate of $3(10^{-2})$/s (10 Hz).

As temperature is increased from a low of −150 °C, EMAA goes through the γ-transition (∼−120 °C) where the storage modulus gradually decreases from about 2.5 to 1.5 GPa. The γ-transition is a low activation energy mechanism associated with the local motions of linear ethylene sequences [10]: it is essentially the same as that found in ethylene homopolymers. At the β′-transition, the storage modulus drops sharply from 1 GPa to 20 MPa over a temperature from −20 °C to 70 °C and will be referred to as the glass transition temperature of this material.

3.1.2. Ethylene 9% methacrylic acid butyl acrylate copolymer (EMAABA)

Fig. 2 shows EMAABA storage modulus, loss modulus, and loss tangent curves as a function of temperature at $6(10^{-2})$/s (10 Hz).

The γ-transition is situated around −120 °C and is correlated to the same motions involved for the γ-peak in EMAA. The β-transition (glass transition) highlighted by the loss tangent occurs around 5 °C. Prior work has affiliated the β peak of EMAA copolymers with a relaxation in the amorphous branched polyethylene phase [10]; hence, we speculate that the β peak here is affiliated with the amorphous branched ethylene butyl acrylate regions.

3.1.3. 53% sodium-neutralized ethylene methacrylic acid butyl acrylate terpolymer ($EMAABA_{Na}$)

Storage modulus, loss modulus and loss tangent curves of the $EMAABA_{Na}$ are shown in Fig. 3 at a converted strain rate of $\sim 6(10^{-2})$/s (10 Hz). After neutralization, a γ transition is still located near −120 °C (the storage modulus gradually decreases from about 3.5 to 1.6 GPa). The β-transition was also little altered upon neutralization: a β transition still occurs at ∼5 °C with the storage modulus dropping sharply from 1.6 GPa to 55 MPa over a temperature from −75 °C to 20 °C and is at the tail end of the leathery regime (i.e., near the rubbery regime) at room temperature. We consider the γ and β-peaks to be affiliated with the same motions and relaxation as for EMAABA.

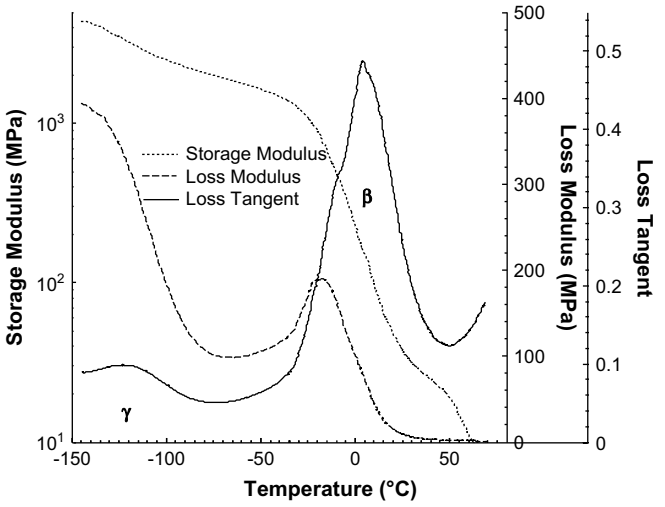

Fig. 2. EMAABA storage modulus, loss modulus, and loss tangent curves as a function of temperature at 10 Hz ($6(10^{-2})$/s).

Fig. 4 compares the loss modulus and storage modulus curves of EMAA, EMAABA and $EMAABA_{Na}$ copolymers. The comparison between loss moduli of unneutralized EMAA, EMAABA and sodium-neutralized EMAABA (Fig. 4a) shows that the γ loss peak is not affected by the addition of butyl acrylate and is independent of neutralization. On the other hand, the butyl acrylate termonomer reduces the glass transition temperature compared to EMAA. Upon neutralization, the β-transition is broadened, occurring over a wide range of temperatures. The $EMAABA_{Na}$ moduli are greater than those of EMAABA at room temperature (also seen in Fig. 4b), reflecting the stiffening effect of the ionic aggregates on the compliant amorphous domains. Hence, neutralization results in a material with enhanced stiffness and enhanced dissipation effective over a wide range of desirable operating temperatures (25 ± 10 °C). Interestingly, the storage modulus of the EMAABA and $EMAABA_{Na}$ in the glassy region of the curves is nearly identical, suggesting that the stiffness of the ionic aggregates must be similar to the glassy modulus of the amorphous domains. Fig. 4b shows that the EMAA storage modulus drops from the glassy regime into the leathery regime at around 30 °C whereas the EMAABA and $EMAABA_{Na}$ drops begin at around −40 °C. Thus, at room

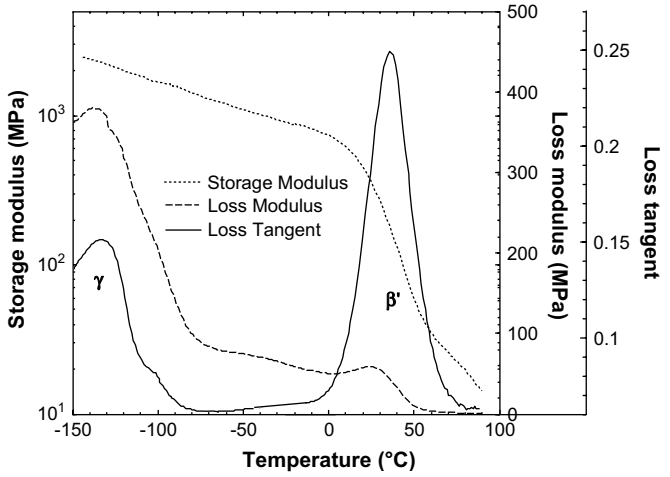

Fig. 1. EMAA storage modulus, loss modulus, and loss tangent curves as a function of temperature at 10 Hz ($3(10^{-2})$/s).

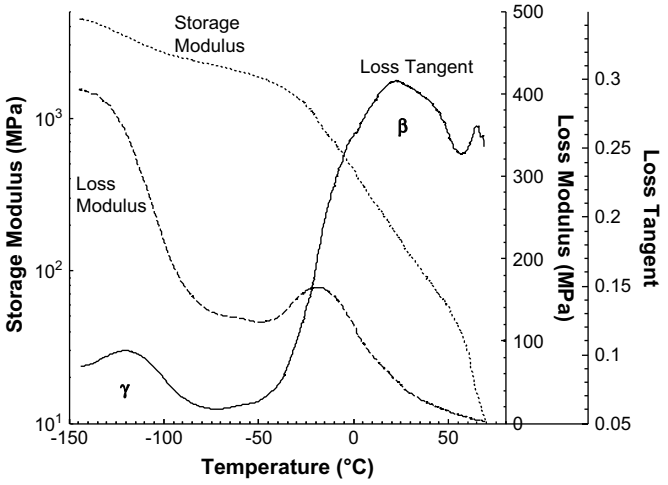

Fig. 3. $EMAABA_{Na}$ storage modulus, loss modulus, and loss tangent curves as a function of temperature at 10 Hz ($6(10^{-2})$/s).

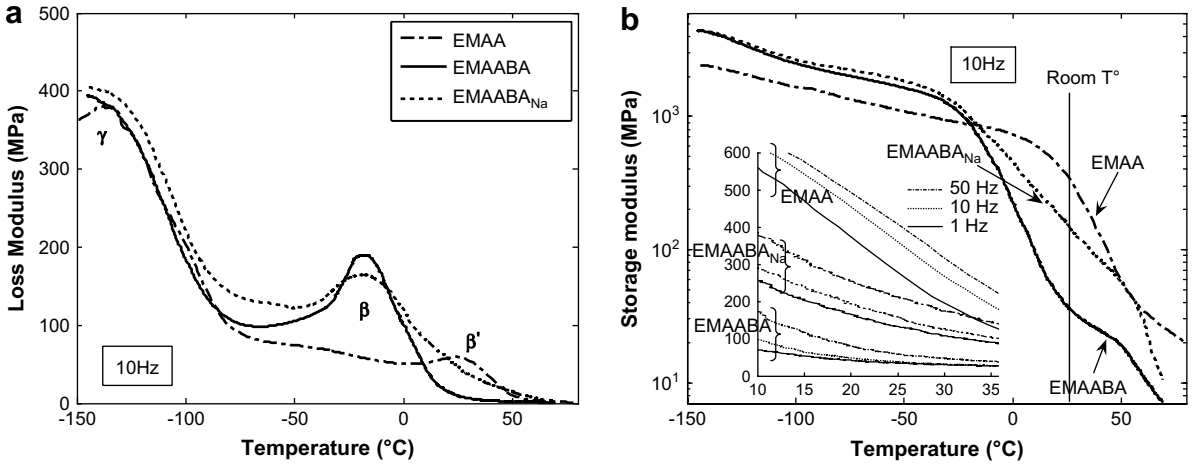

Fig. 4. Comparison between EMAA, EMAABA and sodium-neutralized EMAABA: (a) loss modulus and (b) storage modulus curves as a function of temperature at 10 Hz ($\sim 4(10^{-2})$/s). The inset shows storage modulus curves of EMAA, EMAABA and EMAABA$_{Na}$, around room temperature at 1 Hz ($\sim 4(10^{-3})$/s), 10 Hz ($\sim 4(10^{-2})$/s) and 50 Hz ($\sim 2(10^{-1})$/s), illustrating the shifting of the mechanical behavior with strain rate.

temperature and low rates, EMAA is in the leathery regime but close to the glassy regime, EMAABA$_{Na}$ is well into the leathery regime and EMAABA is nearly beyond the leathery regime and into the rubbery regime.

For room temperature ($\sim$23 °C) behavior, the prominent relaxation mechanism for each of these polymers is the glass transition. The inset in Fig. 4b represents the storage modulus of each material around room temperature, at different frequencies (1 Hz ($\sim 4(10^{-2})$/s), 10 Hz ($4(10^{-2})$/s) and 50 Hz ($2(10^{-1})$/s)) illustrating the shifting in mechanical behavior with strain rate. This shifting of the glass transition with strain rate enables a projection of the shift of the nature of the mechanical behavior with strain rate based on the DMA data up to strain rates of $5(10^3)$/s (note that this thermorheologically simple shift does not adequately account for the shifting of the γ-transition mechanism which shifts in a different manner; however, if properly accounting for the γ-transition, we find that it would not be contributory to the deformation behavior until strain rates greater than $5(10^4)$/s). Based on the shift of the glass transition, EMAA will go from a near-glassy leathery regime behavior at low (10^{-3}/s) rates to a glassy behavior at high (10^3/s) rates; EMAABA will shift from a near rubbery-like behavior at low rates to a leathery behavior at high rates; and EMAABA$_{Na}$ will shift from a mid-region leathery behavior at low rates to a near-glassy leathery behavior at high rates.

3.2. Compression testing: rate dependence of stress–strain behavior

Compression testing was conducted at 26 °C to large strains for a wide range of strain rates (10^{-4}–$6(10^3)$/s) on EMAA, EMAABA and EMAABA$_{Na}$.

3.2.1. EMAA

Fig. 5a shows typical stress–strain curves obtained from the low end of the strain rate window (10^{-4}/s to 10^{-1}/s) through the moderate strain rates (1–10^2/s) to the high rate curves ($2(10^2)$–$6(10^3)$/s).

The stress–strain behavior is highly nonlinear and strongly rate dependent, exhibiting an initially stiff behavior with a rollover to a more compliant behavior at a strain of about 0.10–0.15 followed by a second rollover to an even more compliant behavior at a strain of about 0.40. This "double-yield" phenomenon has been observed in polyethylene materials [22–24] and has been attributed to yield events in the crystalline domains. The stress levels at any given strain increase with strain rate, with the double yield being more apparent at strain rates >1/s. For the moderate to very high rate regime, the initial stiffness region of the curve does not provide accurate data because the force acting on the front side and back side of the specimen does not reach dynamic equilibrium below a strain of ~0.18 for our particular SHPB loading conditions. In Fig. 5b the stress magnitudes for EMAA at different values of true

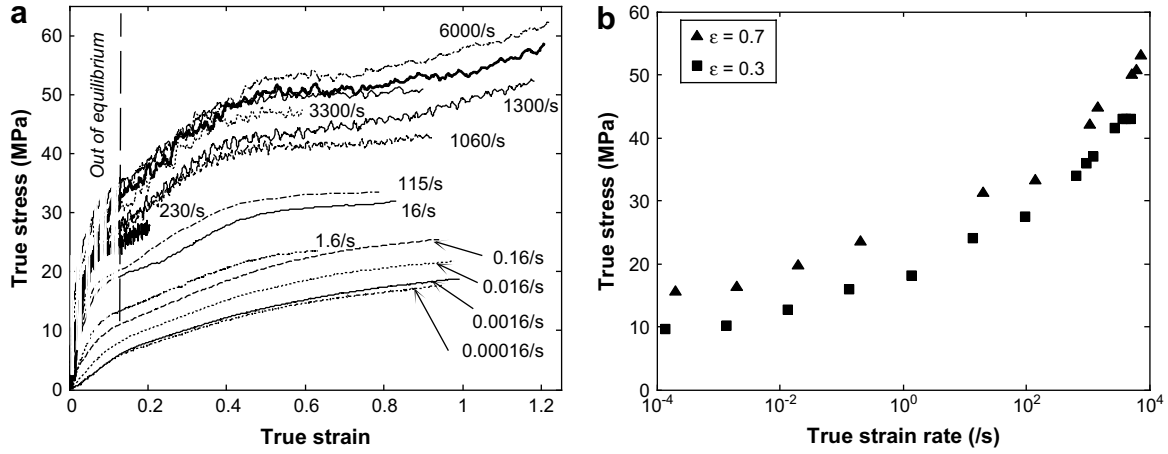

Fig. 5. (a) Uniaxial compression true stress–true strain behavior of EMAA over a wide range of strain rates. (b) Stress as a function of true strain rate at different values of true strain (0.3 and 0.7) for EMAA.

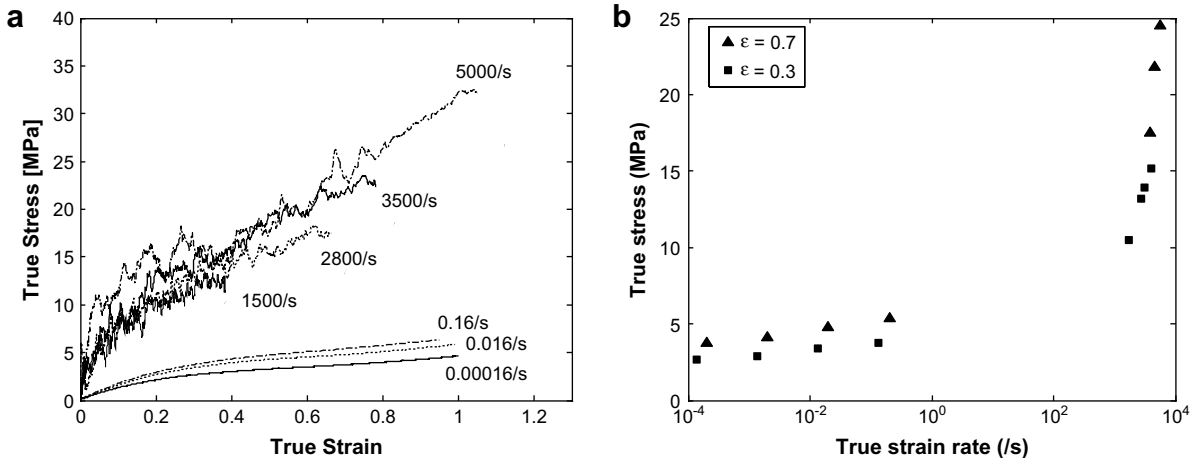

Fig. 6. (a) Uniaxial compression true stress–true strain behavior of EMAABA from low to high strain rates. (b) Stress as a function of true strain rate at different values of true strain (0.3 and 0.7) for EMAABA.

strain are plotted as a function of true strain rate on a logarithmic scale. The stress increases with strain rate over the entire experimental range, with a transition to a region of enhanced strain rate sensitivity appearing around 10/s. This change in rate sensitivity from low to high strain rates is fully consistent with the shifting of the glass transition discussed earlier where at low rates the material is in the near-glassy leathery regime whereas at high rates the material is glassy with a clear yield stress.

3.2.2. EMAABA

The strong rate dependence of the EMAABA large deformation behavior is shown in Fig. 6a. The curves show a relatively stiff initial behavior (albeit considerably less stiff than the EMAA material) followed by a rollover at a strain of about 0.10–0.15 to a more compliant, near constant tangent stiffness behavior up to very large strains. The EMAABA copolymer did not exhibit a double yield.

All features of the stress–strain curve are rate dependent with the stress levels at any given strain increasing with an increase in strain rate. To further assess the rate sensitivity of EMAABA, values of true stress taken at true strains of 0.3 and 0.7 are plotted against their corresponding true strain rate on a logarithmic scale in Fig. 6b. In the low strain rate regime, the EMAABA stress appears to increase approximately linearly with the logarithm of strain, and there is an abrupt change to a much stronger dependence on strain rate in the high rate regime. This change in rate sensitivity from low to high strain rates is fully consistent with the shifting of the glass transition discussed earlier where at low rates the material is near the rubbery end of the leathery regime whereas at high rates the material has fully entered the leathery regime where intermolecular interactions in the amorphous domains begin to pose a significant resistance to deformation.

3.2.3. $EMAABA_{Na}$

Fig. 7 shows the effect of true strain rate (ranging from 10^{-4}/s to $5.5(10^3)$/s) on the true stress–true strain behavior of $EMAABA_{Na}$. The deformation behavior of $EMAABA_{Na}$ exhibits the same basic nonlinear features as the EMAABA; it is also strongly rate dependent and exhibits a rate-sensitivity transition similar to the one for neat EMAABA. Fig. 7b shows again, in the low strain rate regime, the quasi-linear increase of the stress with the logarithm of strain rate and then a transition of the $EMAABA_{Na}$ stress to a stronger dependence on strain rate in the high rate regime. This increase in rate sensitivity occurs at a strain rate of about 10^2/s. This transition in rate sensitivity is also fully consistent with the shifting of the glass transition discussed earlier where from low to high rates the material transitions from the mid-leathery regime to the glassy end of the leathery regime.

Under conditions of very high strain rate loading, any dissipative aspects of the deformation will be manifested as a temperature rise in the specimen since there is insufficient time for any heat transfer to the surroundings. Using the instrumentation developments detailed in Garg et al. [21], the temperature rise during high rate ($\sim 3.4(10^3)$/s) compression was measured (Fig. 8a) showing a rise in temperature of 2.5 °C after a strain of 0.8. As shown in Fig. 8b, the stress–strain history was used to calculate the evolution in total work (ΔW) as a function of strain; the temperature rise ($\Delta\theta$) history was used to calculate the dissipated energy (ΔQ) as a function of strain ($\Delta Q = \rho c_p \Delta\theta$ using the measured density $\rho = 950$ kg/m^3 and heat capacity $c_p = 2650$ J/kg K) and the stored energy ($\Delta U = \Delta W - \Delta Q$). (Note that the work related histories begin at a strain of 0.18 since, as mentioned earlier, the stress–strain curve at high rates is not valid at smaller strains since dynamic equilibrium has not been achieved.) These results indicate that dissipation is from a relatively constant stress level contribution (due to the near linear increase in temperature with strain) likely related to the source of the rollover stress barrier and hence further indicates that the post-rollover stiffening is an elastic (storage) phenomenon.

4. Discussion

Fig. 9 shows the effect of butyl acrylate in EMAA and neutralization in EMAABA on the true stress–true strain behavior at strain rates $1.6(10^{-3})$/s and $3.4(10^3)$/s. It is clear that in the case of compression testing at room temperature, the butyl acrylate increases the material compliance giving a lower initial stiffness, lower rollover stress and lower post-rollover stress levels; furthermore, the EMAABA is found to exhibit a single "yield" event compared to the double yield in EMAA. Differential scanning calorimetry (DSC) showed a degree of crystallinity[1] going from about 30% for the EMAA to about 13% for the EMAABA; the reduced crystallinity content is consistent with the loss of the double-yield behavior. Sodium neutralization of EMAABA in turn produces a behavior with a greater initial stiffness, greater rollover stress and greater post-rollover stress level compared to the unneutralized EMAABA. DSC measurements showed very little variation in crystallinity between EMAABA and $EMAABA_{Na}$. Thus we infer that the

[1] Weight fraction crystallinity is calculated by dividing the material's heat of fusion ΔH_f, obtained by differential scanning calorimetry (DSC), by 278 J/g for 100% crystalline polyethylene [25].

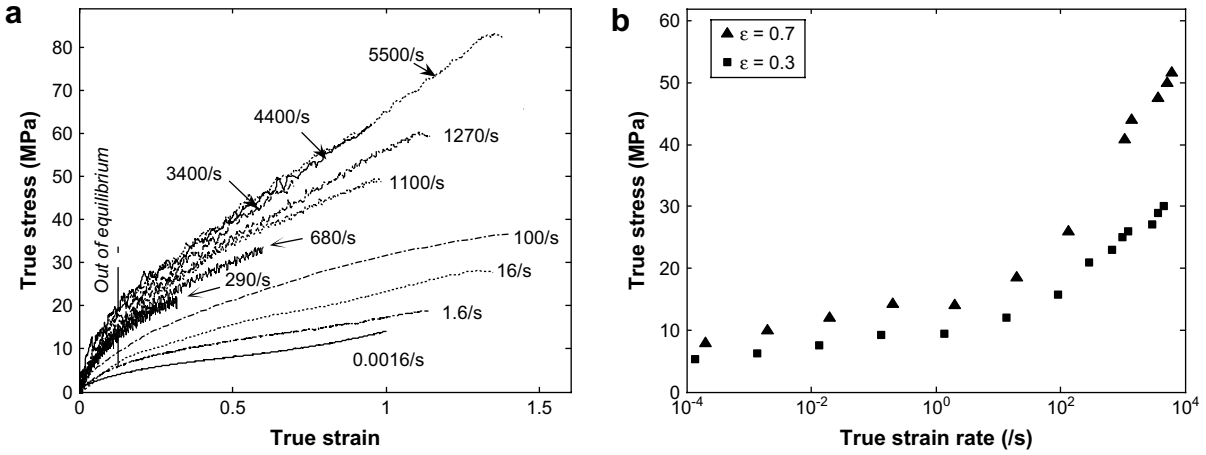

Fig. 7. (a) Uniaxial compression true stress–true strain behavior of $EMAABA_{Na}$ over a wide range of strain rates. (b) Stress as a function of true strain rate at different values of true strain (0.3 and 0.7) for sodium-neutralized EMAABA.

observed stiffening resulting from neutralization of EMAABA is not due to the change in crystallinity but instead results from the presence of stiff ionic aggregates within the amorphous domains and widening of the glass transition regime upon Na neutralization. Overall, the changes in room temperature stress–strain behavior are consistent with the locations of the glass transition temperatures of these materials as seen in the DMA data as shown, for example, in the direct comparison of the storage moduli of the three materials in Fig. 9b.

Fig. 10 presents the rate dependence of the stress–strain behavior of EMAA, EMAABA and $EMAABA_{Na}$ in the form of true stress versus logarithm of strain rate, taking the stresses evaluated at a strain level of 0.3. For each copolymer, the data over the wide strain rate range (almost 8 orders of magnitude in strain rate) show a logarithmic dependence on strain rate at low rates and a departure from this dependence at a moderate rate (the departure rate is dependent on the polymer). The change in rate sensitivity for each polymer is consistent with its transitioning through its respective glass transition regime as discussed earlier and quantified in the DMA data.

5. Modeling

Constitutive models able to capture the stress–strain behavior of amorphous polymers over a wide range of strain rate have recently been developed for several polymers including polycarbonate [19,26], polymethylmethacrylate [19,26], polyvinyl chloride [18] and thermoplastic olefin [18,19,26,27] and follow a Ree–Eyring [28] multiple process model building on work of Bauwens-Crowet et al. [29]. A fundamental assumption recurring in all these models is that the stress response can be decomposed into multiple mechanisms. The multiple mechanisms may be due to multiple relaxation processes in the polymer (for example, contributions from both primary and secondary transitions in polycarbonate [19,26]) or from relaxation mechanisms in each phase of a multi-phase polymer [27]. Recently, Scogna and Register [30] showed that the yield stress of EMAA copolymers can be described by the sum of contributions from two mechanisms, crystal slip in the crystalline domains and a second mechanical relaxation in the non-crystalline domains. Here, we recognize the two-phase structure of these copolymers (hard domains and amorphous domains) and consider a three mechanism model for the stress–strain behavior:

- Mechanism H represents the resistance due to yield in the hard domains; morphologically we consider the hard domains to primarily consist of crystalline regions in the materials studied here.
- Mechanism A represents the resistance due to the intermolecular interactions within the amorphous domains. This resistance is negligible above the glass transition temperature. However, as the temperature decreases (or rate increases) and

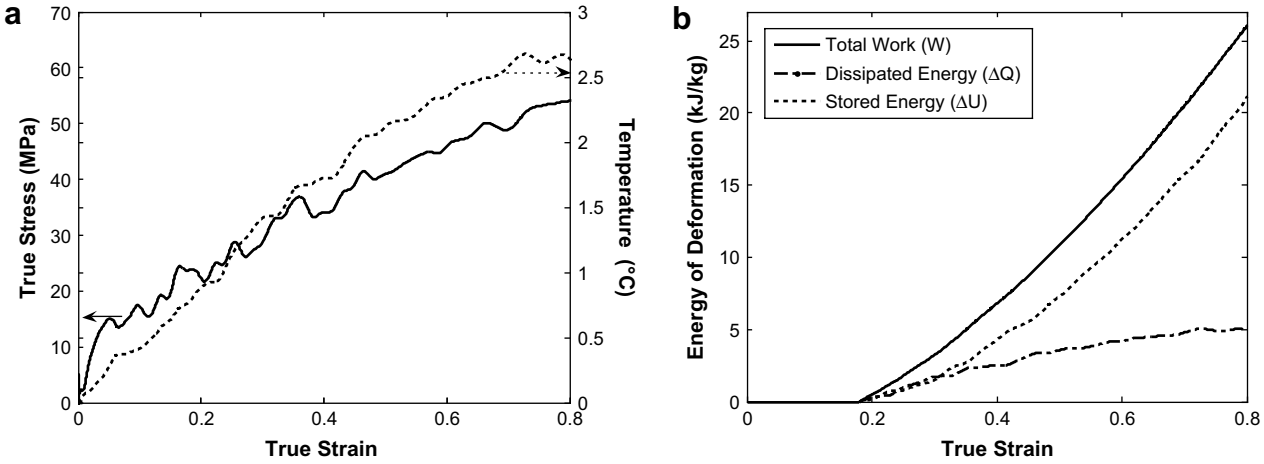

Fig. 8. (a) True stress and rise in temperature of $EMAABA_{Na}$ as a function of strain during adiabatic compression at a strain rate of $\sim 3.4(10^3)$/s. (b) Total work, dissipated and stored energy as a function of strain as reduced from the stress–strain and temperature rise–strain data.

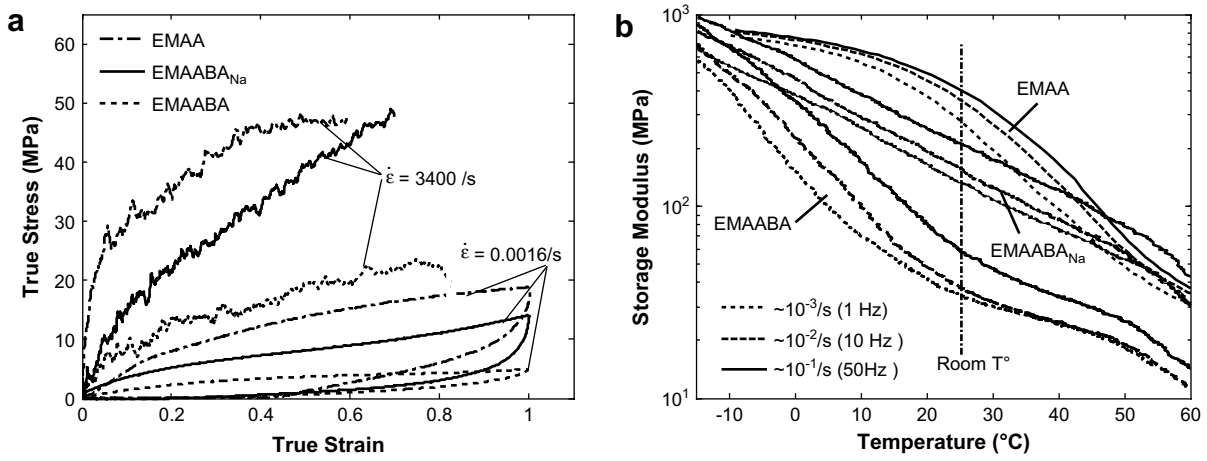

Fig. 9. (a) True stress–true strain behavior of EMAA, EMAABA and EMAABA$_{Na}$ in compression testing at 1.6(10^{-3})/s and 3.4(10^{3})/s true strain rate and (b) shifting effect with strain rate: storage modulus of EMAA, EMAABA and EMAABA$_{Na}$ at ~10^{-3}/s, ~10^{-2}/s and 10^{-1}/s.

the material transitions down through the glass transition, the intermolecular interactions become significant and this resistance is no longer negligible.

- Mechanism N represents the network resistance due to stretching and orientation of the molecular network. This molecular network exists in the amorphous zones of the various materials and consists of trapped and untrapped entanglements of the chains that thread through the crystalline and amorphous domains mentioned above.

Thus, at the selected temperature and strain rate, the total stress acting on the copolymer is given by the sum of the stress contributions from the three mechanisms,

$$\sigma = v_H\sigma_H + v_A(\sigma_A + \sigma_N)$$

where v_H and v_A are the effective volume fractions of the hard and amorphous domains, respectively. Since some of the amorphous domains are trapped among the hard domains and cannot deform, the effective volume fraction of hard domains is larger than the physical fraction [31,32]. Here the effective volume fraction of the hard domains is taken to be 10% larger than the physical volume fraction. The EMAA material was found to have 30% crystallinity content as compared to 13% for the EMAABA materials, so that for EMAABA materials v_H and v_A are equal to 0.23 and 0.77 respectively, whereas for EMAA they are 0.4 and 0.6, respectively. At each strain rate the contribution to the total stress due to mechanism N ($v_A\sigma_N$) is experimentally determined using the post-rollover slope of the stress–strain curve, as depicted in Fig. 11a for the compression tests of EMAABA$_{Na}$ at strain rates of 10^{-1}/s and 3.4(10^{3})/s. For EMAA, the value for σ_N at a strain of 0.3 was obtained taking the product of the post-rollover slope and the 0.3 strain. The network stress $v_A\sigma_N$ is then subtracted from the total stress σ to give the net contribution of mechanisms H and A ($v_H\sigma_H + v_A\sigma_A$) as shown in Fig. 11b–d, where the stress is plotted against the logarithm of the strain rate for EMAA, EMMABA and EMMABA$_{Na}$, respectively.

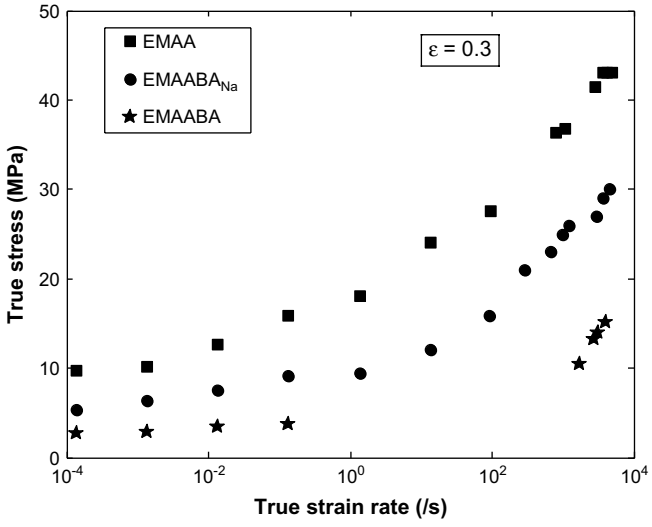

Fig. 10. Effect of butyl acrylate and sodium neutralization in EMAA on the evolution of true stress versus true strain rate at 0.3 strain.

The contributions from mechanisms H and A may each be represented using the Ree–Eyring model [28],

$$\frac{\sigma_i}{T} = \frac{R}{v_i}\sinh^{-1}\left[\frac{\dot{\varepsilon}}{\dot{\varepsilon}_i^0}\exp\left(\frac{\Delta H_i}{RT}\right)\right], \quad i = H, A$$

where σ_i is the stress from the "i" process, R is the gas constant, v_i is the activation volume, $\dot{\varepsilon}$ is the applied strain rate, $\dot{\varepsilon}_i^0$ is a constant pre-exponential factor and ΔH_i is the activation energy.

Material properties are obtained by careful reduction of the data. First, we note that at low rates, EMAABA is above its glass transition temperature and hence its flow stress is dominated by the "H" process and properties for the H-process are thus fit to the low strain rate data of EMAABA. Properties for the amorphous domain "A" process of EMAABA are then fit to the high strain rate data (after removal of the H-process contribution via extrapolation of the low strain rate data). The resulting two-process model is then assembled and is shown to provide the excellent fit to the EMAABA data shown in Fig. 12a with the properties listed in Table 1. The EMAABA$_{Na}$ is then fit by first assuming that the hard domain behavior is identical to that of the EMAABA (i.e., the hard domain is taken to be relatively unaffected by neutralization); properties for the A process are then obtained by fitting to the high rate data (after removal of the extrapolated low rate contribution). The strong and changing rate dependence of the EMAABA$_{Na}$ is also found to be well-captured by the two-process model as shown in Fig. 12a. For EMAA materials the same hard domain properties as for EMAABA materials are used as listed in Table 1 and the scaling in stress level is given by the different crystallinity content. The A-process properties were then obtained by fitting to the high rate data after removal of the model predicted extrapolation of the low rate

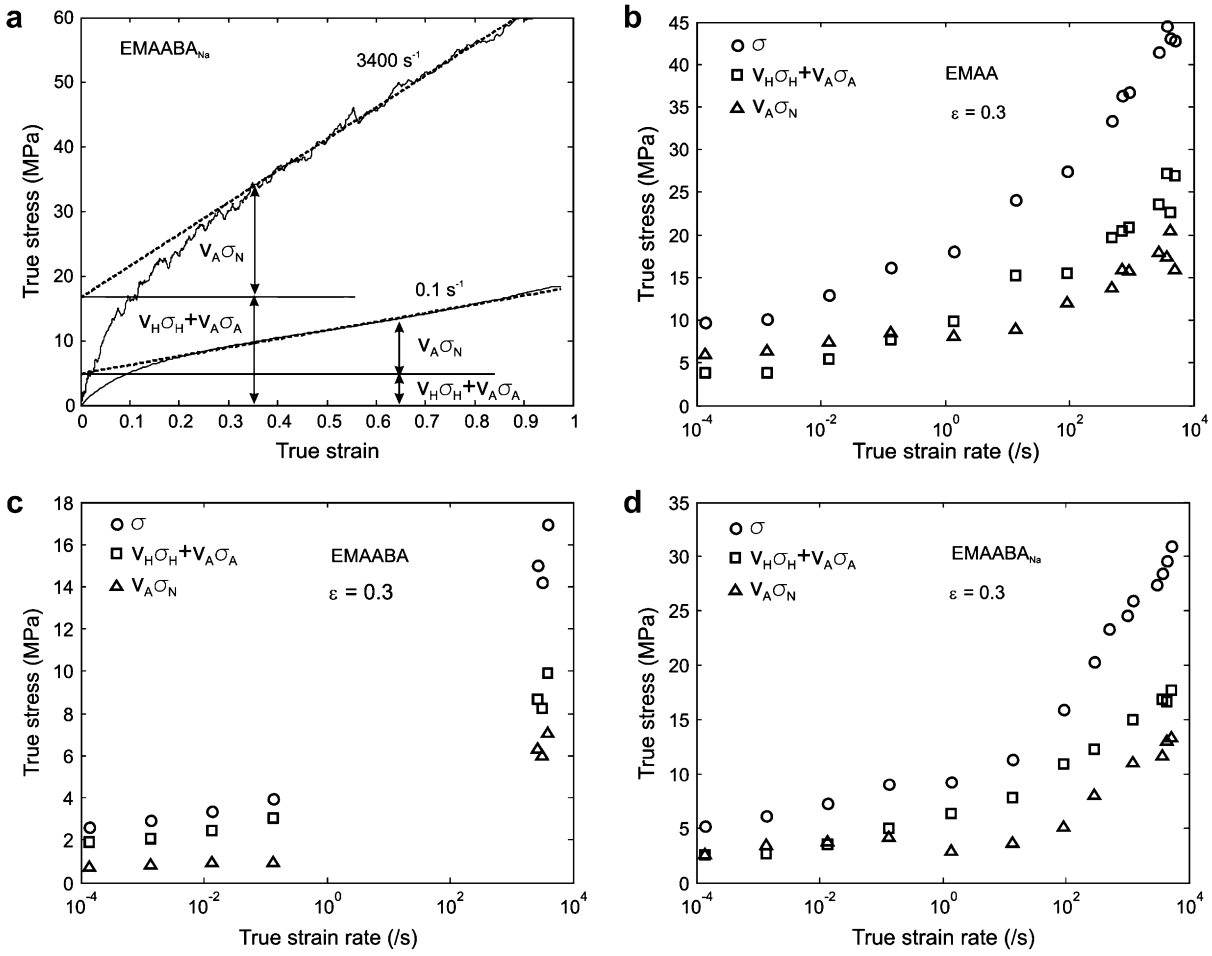

Fig. 11. (a) Stress contributions from mechanisms N, H and A for EMAABA$_{Na}$ at 10^{-1}/s and 3.4(10^3)/s. The post-rollover linear fit lines are shown to demonstrate the method for determining σ_N. (b) Stress decomposition into σ_H, σ_A and σ_N as a function of true strain rate at a true strain of 0.3 for EMAA. (c) Stress decomposition into σ_H, σ_A and σ_N as a function of true strain rate at a true strain of 0.3 for EMAABA. (d) Stress decomposition into σ_H, σ_A and σ_N as a function of true strain rate at a true strain of 0.3 for EMAABA$_{Na}$.

contribution. The comparison between the predictions of the model and the experimental data is reported in Fig. 12, revealing the capability of the two-process flow (yield) stress model to capture the strong and changing rate dependent flow stress (Fig. 12a). For all three materials, the addition of the third deformation mechanism (the network orientation stress) to the two-process model predictions captures the overall stress level and its rate dependence (Fig. 12b). We do note that there are additional complexities to the post-rollover stress–strain behavior of these copolymers including, for example, a softening of the stress–strain

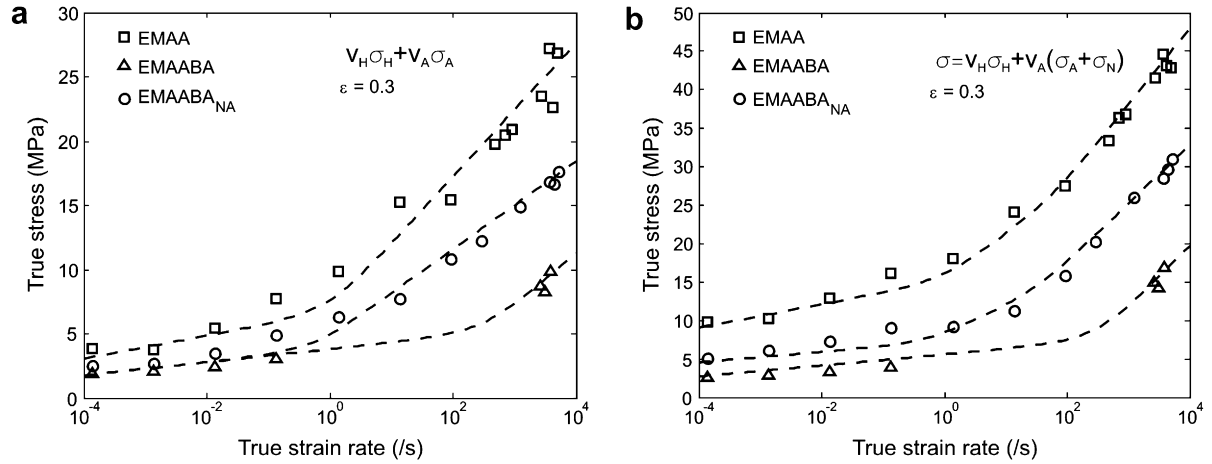

Fig. 12. (a) Calculated model fit (dashed lines) and experimental data (markers) for $\sigma_H+\sigma_{HA}$ as a function of true strain rate at 0.3 true strain for EMAA, EMAABA and EMAABA$_{Na}$. (b) Calculated model fit (dashed lines) and experimental data (markers) for σ as a function of true strain rate at 0.3 true strain for EMAA, EMAABA and EMAABA$_{Na}$. The model results are obtained by adding the experimental value of σ_N to the model results of the $\sigma_H+\sigma_A$.

Table 1
Model best-fit parameter values.

	EMAA	EMAABA	EMAABA$_{Na}$
v_H [nm^3/segment]	4.3	4.3	4.3
$\dot{\varepsilon}_H^0$ [/s]	10^{20}	10^{20}	10^{20}
ΔH_H [kJ/mol]	155	155	155
V_A [nm^3/segment]	1.3	2.1	2.5
$\dot{\varepsilon}_A^0$ [/s]	10^{14}	10^{14}	10^{14}
ΔH_A [kJ/mol]	78.5	64	80

behavior that is evident during unload–reload cycles and address these features in other work [33].

6. Conclusions

The rate dependent behaviors of an ethylene methacrylic acid (EMAA) copolymer, an ethylene methacrylic acid butyl acrylate (EMAABA) copolymer and a sodium-neutralized ethylene methacrylic acid butyl acrylate (EMAABANa) ionomer have been investigated over eight orders of magnitude in strain rate in the region around the glass transition of the materials. The true stress–true strain behavior of each polymer exhibits a nonlinear response characterized by an initially relatively stiff response, to a clear rollover at a strain of ~0.10 to 0.15, to a more compliant tangent stiffness. The stress levels at any given strain are found to increase with an increase in strain rate. Plots of stress versus logarithm of strain rate revealed the nature of the rate dependence to change with strain rate, exhibiting an enhanced dependence on strain rate at high rates, for each polymer. This change in rate dependence is a more gradual phenomenon for EMAA since the EMAA storage modulus transitions from the glassy end of the leathery regime at low rates to entering the glassy regime at high strain rates (Fig. 4b). On the other hand, the change in rate sensitivity is more distinct for EMAABA and EMAABA$_{Na}$ (as evidenced by a distinct departure from logarithmic dependence at low rates) and is consistent with a transition within the leathery regime where there is a more dramatic changing of intermolecular interactions with increasing rate: from the rubbery end of the leathery regime at low rates to fully into the leathery regime with increasing strain rate for EMAABA and from a mid-leathery behavior at low rate to a nearer glassy end of the leathery regime for the EMAABA$_{Na}$. Furthermore, the unneutralized EMAA possesses a relatively high modulus (Fig. 4) since it is near the glassy end of the leathery regime and the amorphous regions are not fully relaxed. On the other hand, for EMAABA, the butyl acrylate content reduces the β (glass transition) temperature and thus, the amorphous regions are relaxed during room temperature measurements, leading to a lower room temperature modulus (Fig. 4). Furthermore, the room temperature modulus of the neutralized EMAABA, observed in Fig. 4, is greater than the EMAABA likely as a result of stiffening from ionic aggregates and the glass transition is broadened. The transitioning in the rate dependence of the flow stress of each material is successfully emulated using a two-process Ree–Eyring representation of flow with one process capturing the rate dependence of the resistance of the hard (crystalline) domains and the second process capturing the resistance of the intermolecular interactions of the amorphous domains; the amorphous domain resistance is strongly dependent on strain rate due to the proximity to the glass transition and hence governs the observed transition in the rate sensitivity of the mechanical behavior of these polymers.

Acknowledgments

This research was sponsored by the DuPont MIT Alliance program. We appreciate numerous technical discussions with D.E. Spahr, K.R. Samant, W. Marsh of DuPont. The authors also thank Dr. Bo Song for his assistance through training in the use of equipment at Purdue University.

References

[1] MacKnight WJ, Earnest TR. Journal of Polymer Science: Macromolecular Reviews 1981;16:41–122.
[2] Tant MR, Wilkes GL. Journal of Material Science, Macromolecular Chemistry and Physics C 1988;28:1.
[3] Kinsey RH. Applied Polymer Symposia 1968;11:77–94.
[4] Eisenberg A, Kim J. Introduction to ionomers. New York: John Wiley & Sons, Inc.; 1998.
[5] Eisenberg A, Hird B, Moore RB. Macromolecules 1990;23:4098–107.
[6] Yarusso DJ, Cooper SL. Macromolecules 1983;16:1871–80.
[7] Ng CWA, MacKnight WJ. Macromolecules 1996;29:2421.
[8] Eisenberg A. Macromolecules 1970;3:147.
[9] Delf BW, MacKnight WJ. Macromolecules 1969;2:309–10.
[10] MacKnight WJ, McKenna LW, Read BE. Journal of Applied Physics 1967; 38(11):4208–12.
[11] Tachino H, Hirasawa E, Kutsumizu S, Tadano K, Yano S. Macromolecules 1993; 26:752–7.
[12] Khanna YP, Wenner WM, Krutzel L. Macromolecules 1988;21:268–70.
[13] Hirasawa E, Yamamoto Y, Tadano K, Yano S. Journal of Applied Polymer Science 1991;42:351–62.
[14] Wakabayashi K, Register RA. Macromolecules 2006;39:1079–86.
[15] Akimoto H, Kanazawa T, Yamada M, Matsuda S, Shonaike G, Murakami O. Journal of Applied Polymer Science 2001;81:1712–20.
[16] Ehrlich P, Mortimer G. Fortschritte der Hochpolymeren-Forschung 1970:386–448.
[17] Woodbrey JC, Ehrlich P. Journal of the American Chemical Society 1963; 85(11):1580–4.
[18] Soong SY, Cohen RE, Boyce MC, Mulliken AD. Macromolecules 2006; 39(8):2900–8.
[19] Mulliken AD, Boyce MC. International Journal of Solids and Structures 2006; 43(5):1331–56.
[20] Sarva SS, Deschanel S, Boyce MC. Polymer 2007;48:2208–13.
[21] Garg M, Mulliken AD, Boyce MC. Journal of Applied Mechanics 2008; 75(1):011009.
[22] Brooks NWJ, Duckett RA, Ward IM. The Society of Rheology, Inc. Journal of Rheology 1995;39:425–36.
[23] Brooks NWJ, Unwin AP, Duckett RA, Ward IM. Journal of Macromolecular Science, Part B 1995;34(1 & 2):29–54.
[24] Foot JS, Truss RW, Ward IM, Duckett RA. Journal of Materials Science 1987; 22:1437–42.
[25] Wunderlich B. Macromolecular physics. New York: Academic Press; 1973.
[26] Richeton J, Ahzi S, Daridon L, Rémond Y. Polymer 2005;46(16):6035–43.
[27] Wang Y, Arruda EM. Journal of Engineering Materials and Technology 2006;128(4):551–8.
[28] Ree T, Eyring H. Journal of Applied Physics 1955;26(7):793–800.
[29] Bauwens-Crowet C, Bauwens JC, Homès G. Journal of Polymer Science, Part A-2: Polymer Physics 1969;7(4):735–42.
[30] Scogna RC, Register RA. Polymer 2008;49(4):992–8.
[31] Bergström JS, Boyce MC. Rubber Chemistry and Technology 1999;72(4): 633–56.
[32] Medalia AI, Kraus G. In: Mark JE, Erman B, Eirich FR, editors. Science and technology of rubber. New York: Academic Press; 1994. p. 387–418.
[33] Bertoldi K, Greviskes BP, Deschanel S, Cohen RE, Boyce MC, in preparation.